GAMMA RADIATION SCATTERING AND ATTENUATION PROPERTIES OF BARYTES CONCRETE

by

Walid Constantine Assaf

A Thesis Submitted to the
Graduate Faculty in Partial Fulfillment of
The Requirements for the Degree of
MASTER OF SCIENCE

Major Subject: Nuclear Engineering

Approved:

Iowa State University
Of Science and Technology
Ames, Iowa

1962

TABLE OF CONTENTS

INTRODUCTION

The problem of scattering and absorption of gamma rays has occupied many investigators for over half a century. Some of the theoretical aspects of scattering and absorption of these rays have been discussed by Compton (3), Fermi (5), Green (9) and Heitler (11). Even though theory is well developed and completely describes the interactions of gamma rays with matter, it leaves much to be desired when practical problems arise in shielding of nuclear reactors and other sources of radiation (1, 7, 10). The difficulty arises from the fact that theory develops relations on the basis of single interactions between a photon and an electron and it does not account for such factors as buildup and multiple scattering.

In this investigation, an attempt has been made to find the extent of such complications in scattering for a barytes concrete block measuring 2x2x4 inches. Particular attention was given to the scattered radiation emerging from the corners of the block. This was done in order to determine if the presence of the corner had any effects on the multiplicity of such scattering.

REVIEW OF LITERATURE

Interactions of Gamma Rays with Matter

Gamma radiation is the name given to the electromagnetic radiation originating at excited nuclei of some radioactive materials. Gamma rays are identical with X rays and the two cannot be distinguished from each other. The only difference between the two comes from the fact that X rays have their origin at the electronic shells of an atom when the electrons undergo changes in energy states, while gamma rays are emitted directly from changes in energy states in the nucleus. Figure 1 displays the electromagnetic spectrum of radiation in terms of photon energy and frequency in cycles per second (13). Since gamma radiation occurs at the higher end of the spectrum in terms of frequency and energy, its effects on humans as well as materials become damaging. This is to be contrasted with the essentially harmless radio waves that fill the air.

Due to this fact the detection and evaluation of gamma ray interaction with matter has occupied many investigators for over half a century.

In the follcwing pages an attempt has been made to summarize some important aspects of gamma rays with emphasis on their scattering properties. For more detailed analysis of the penetration of gamma rays, the reader might refer to Avery (1), Grotenhuis (10), Goldstein (7) and Ruddy (19).

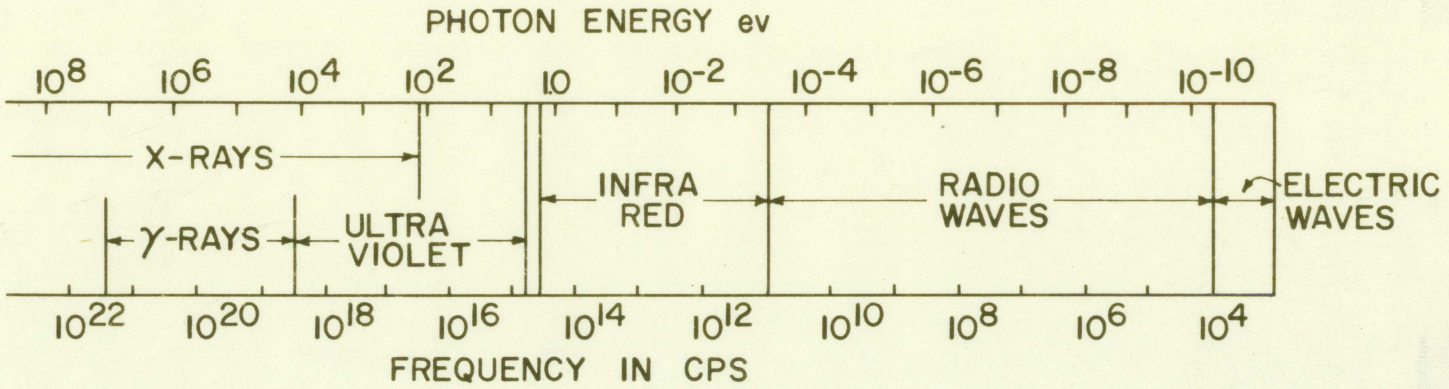

Figure 1. The electromagnetic spectrum on a logarithmic frequency (Energy) scale

There are three primary mechanisms by which photons of gamma radiation are either absorbed or scattered.

Photoelectric absorption

The electrons which surround the nucleus are grouped according to their binding energies into the K, L, M, N shells. When the frequency (ν) of the incident photon is increased from zero, its energy, which is given by the expression

$$E = h\nu$$

where

h = Plancks' constant and

$\nu = c/\lambda$

c = speed of light

λ = wave length of the incident photon,

reaches a value corresponding to the binding energy of electrons in the K and L shells (5) where a large absorption of photon energies occurs. This absorption removes an amount of energy from the incident beam equal to the binding energy of the electron in addition to any kinetic energy that may be imparted to the electrons. This may be represented by the equation

$$h\nu = K.E. + K_{ab}$$

where

$h\nu$ = energy of the incident photon

K.E. = kinetic energy of the ejected electron

K_{ab} = binding energy of an electron in the K shell.

The energy removed from the incident photon by photoelectric absorption is complete, a fact which requires this interaction to take place with a bound K or L electron where the atom and the ejected electron can conserve momentum (4).

Compton scattering

When the energy of the incident photon is large compared with binding energy of the electrons, such electrons may be considered as free electrons rather than bound as was the case in the photoelectric effect.

The process giving rise to scattering of photons by a free electron may be described in the following manner.

An incident photon of energy E_o collides with a free electron which may be assumed to be initially at rest. The scattered photon emerges at energy E^1 less than E_o. In this interaction it has been demonstrated that momentum is conserved (11) and that the energy of the incident photon is related to the energy of the scattered photon and its angle of scatter by the equation

$$E^1 = \frac{E_o}{1 + \frac{E_o}{mc^2}(1 - \cos\theta)}$$

where mc^2 is the rest energy of the electron which is equal to

.51 mev. (Heitler).

In general, Compton scattering involves the outermost electrons surrounding the atom. It therefore does not produce any significant interactions with K or L electrons (4).

In addition to the above Compton formula which describes the angular distribution of the scattered radiation, Klein and Nishina (9) derived the following expression for the differential cross section of an unpolarized incident beam of photons.

$$\sigma_c(\theta,\phi) = \frac{3\sigma_e}{16\pi} \frac{1+\cos\theta}{[1+\varsigma(1-\cos\theta)]^3}\left\{1+\frac{\varsigma^2(1-\cos\theta)^2}{(1+\cos^2\theta)[1+\varsigma(1-\cos\theta)]}\right\}$$

where

$\sigma_c(\theta,\phi)$ = differential cross section per unit solid angle in cm^2/electron for the number of photons scattered in the direction , and

$$\varsigma = \frac{Er}{mc^2}$$

where

Er = incident gamma ray energy mev.

The Klein-Nishina cross sections have been plotted for an energy range of 10 kev to 500 mev by Nelms (16). One such plot is reproduced in Figure 2. Figure 3 shows the same cross section for 1.25 mev incident photon energy, plotted on polar coordinates.

For an incident photon of energy in the range of 1 mev,

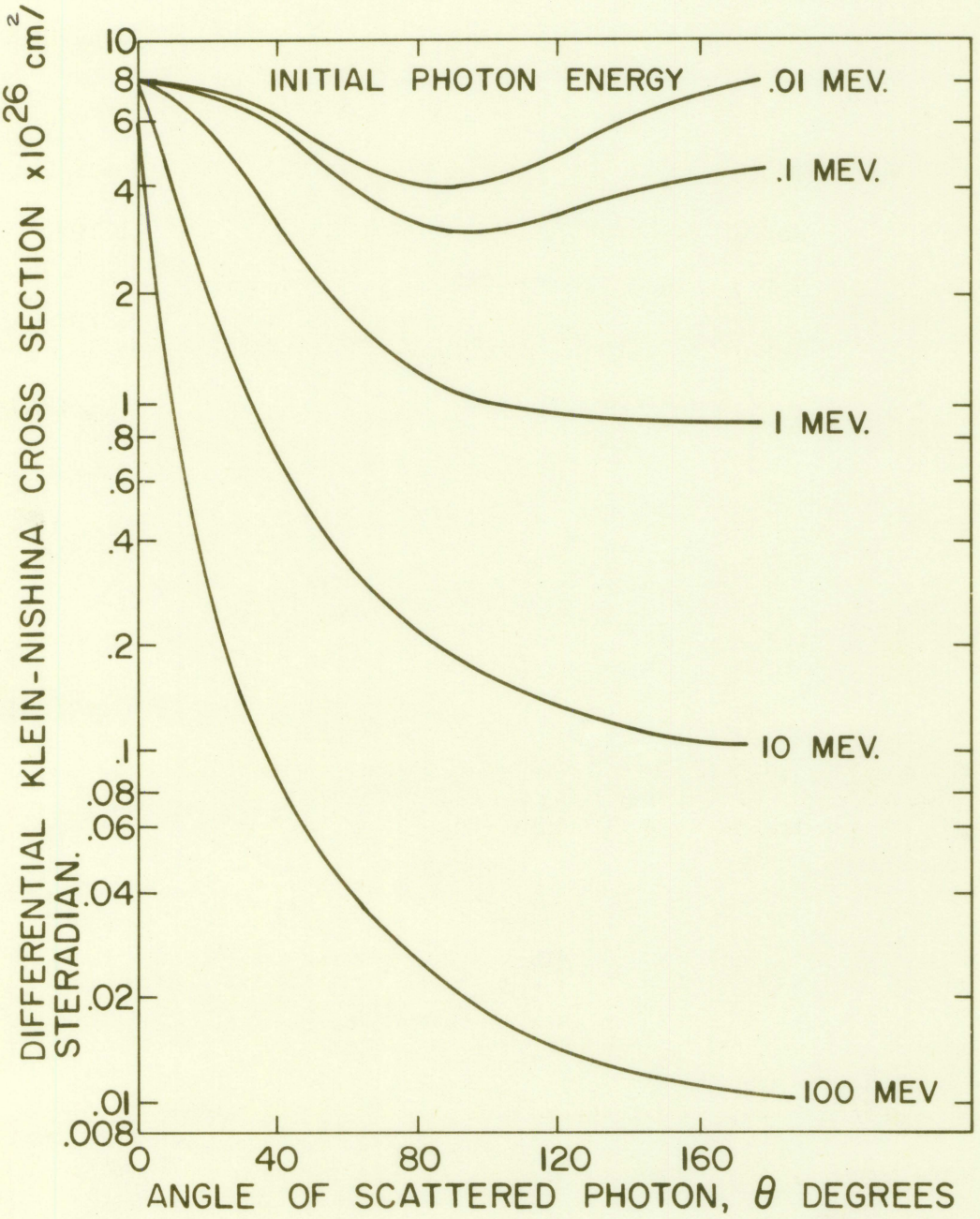

Figure 2. The Klein-Nishina cross section as a function of angle and energy of the incident photon

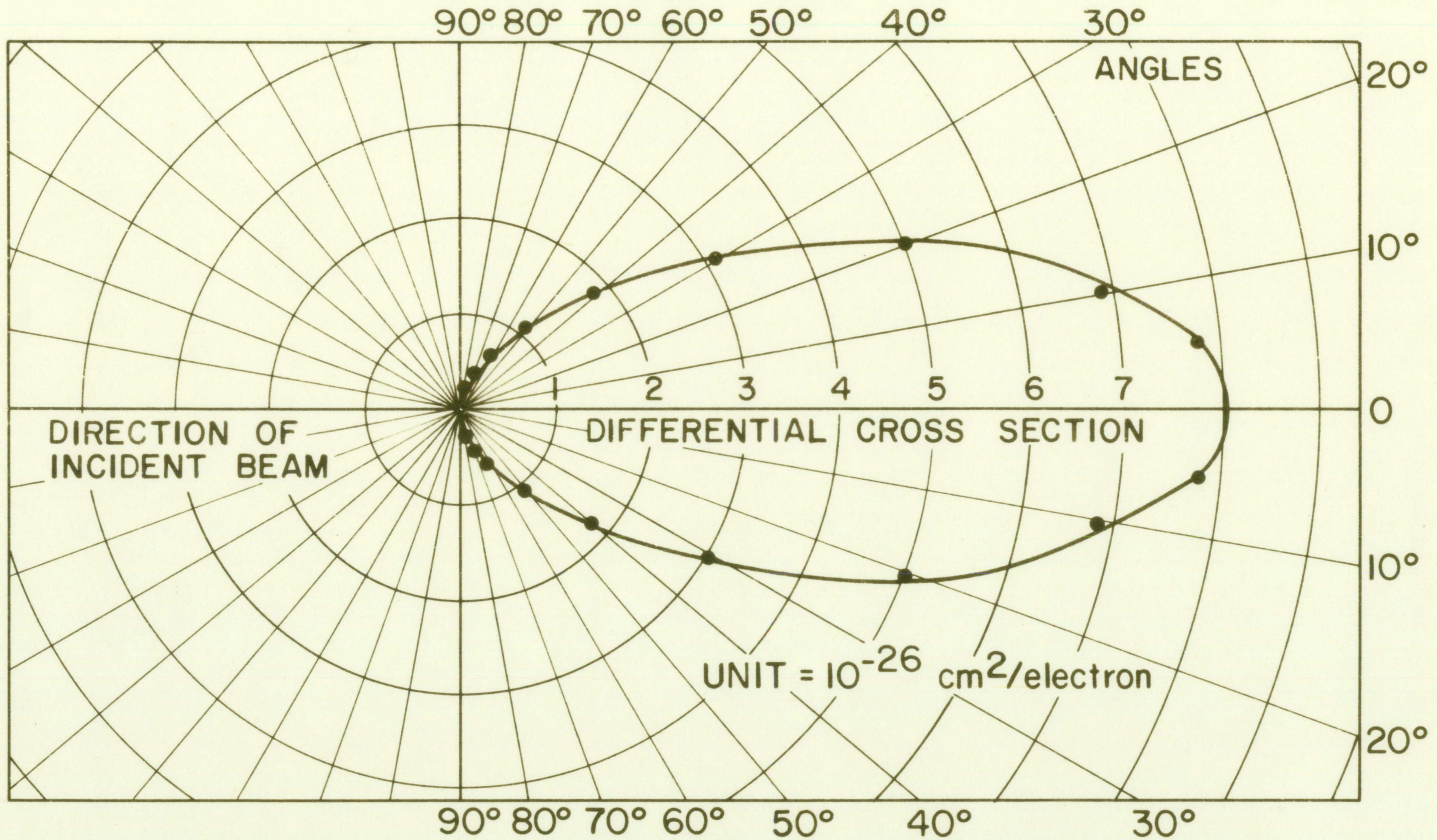

Figure 3. The Klein-Nishina distribution as a function of the scatter angle

the differential cross section shows a uniform drop from 40° to 80°, a fact which will be compared to the results of this investigation.

Pair production

For higher photon energies pair production becomes of increasing importance in absorption of gamma ray radiation (5). Here a gamma photon disappears and a positron-electron pair is produced. The condition giving rise to this absorption may be summarized by stating that when a photon passes near an atomic nucleus, the strong electric field in that vicinity converts the gamma photon into an electron-positron pair which requires $2m_0c^2$ for its formation (17).

From this it can be seen that for every event leading to pair production the incident beams suffer a loss of energy equal to at least $2m_0c^2$ or 1.02 mev.

For a clear understanding of this mechanism of absorption, quantum mechanics methods must be considered. This has been done in Heitler (11).

Mass Absorption Coefficient

The mass absorption coefficient usually given in cm^2/gm is defined as the fraction of photons not absorbed after having passed a distance X of some absorber (5). The distance X is given in gm/cm^2.

If an incident beam of radiation is represented by the

intensity I_o and the emerging beam by I, then the fraction of radiation not absorbed is I/I_o. This fraction is related to the mass absorption coefficient by the equation

$$\frac{I}{I_o} = e^{-\mu_m X}$$

where μ_m is the mass absorption coefficient defined above and X is the modified distance term obtained by multiplying the actual thickness of absorber, x, by its density. The units used must of course be consistent.

A relation between the mass absorption coefficient and the cross section per atom (5) may be derived as follows:

Given: An incident beam of gamma photons, I_o per cm^2 second falling on area, a, of thickness, dx,

assume that an area B within, a, absorbs all of the incident photons. B is then defined by

$$\frac{\sigma\ cm^2}{Atom} \left| \frac{N\ atoms}{cm^3} \right| a\ dx\ cm^3$$

$$B = Nadx.$$

The number of photons absorbed per second is given by $I_o(B/a)$ where B/a is the fraction of total effective absorbing area to the total area, a, which the beam strikes.

By making a photon balance i. e. photon in = photon out + absorption, we have

$$I_o = I + I_o(B/a)$$

or $$I_o = I + I_o \frac{\sigma N a dx}{a} ;$$

therefore, $$I_o = I + I_o \sigma N dx.$$

Rearranging this we have

$$\frac{I_o - I}{I_o} = \sigma N dx = \text{fraction absorbed.}$$

The last equation may be written in differential form

$$\frac{dI}{I} = -\sigma N dx$$

where dI is the change in photon flux. Integrating this we have

$$\frac{I}{I_o} = e^{-\sigma N x}$$

which is the fraction not absorbed. The number of atoms is given by the relation

$$N = \left| \frac{\rho \text{ gm}}{\text{cm}^3} \right| \left| \frac{\text{gm-atom}}{A \text{ gm}} \right| \left| \frac{\text{No atoms}}{\text{gm-atom}} \right| ;$$

therefore, $$\frac{I}{I_o} = e^{-\frac{\sigma N_o}{A} \rho x}$$

or $$\frac{I}{I_o} = e^{-\sigma \frac{N_o}{A} X}$$

The above equation may be written in the form

$$\frac{I}{I_o} = e^{-\mu_m X}$$

by analogy with what was stated before where

$$\mu_m = \sigma \frac{N_o}{A}$$

The cross section σ can be calculated for any specific mechanism of absorption or scatter, such as photoelectric absorption, pair production and so on. When σ is a composite of such mechanisms it is called the total cross section per atom and μ becomes the total mass absorption coefficient.

Barytes Concrete as a Shielding Material

When the shielding of gamma rays is considered, we find that only those materials that have a high atomic number (Z) are truly effective in reducing the strength of these highly penetrating rays. Lead, which has an atomic number of 82, has been one of the primary gamma ray shielding materials. However, when a wall 15, 25 or 30 feet high is required for shielding as well as for structural strength, lead fails to

remain a very useful or practical material to use.

Steel, while having the structural strength, lacks the property of easy workability. Therefore its use as a substitute for lead reaches a practical limit of design requirements beyond which it renders itself useless.

Under such conditions the utilization of concretes becomes significant. Stone, sand and cement are available almost anywhere. This, along with the ease with which concrete can be made to fit a variety of shapes, makes it a very attractive and relatively inexpensive material with which to work (12, 20). Its only disadvantage is the great thickness that is required for the adequate shielding of strong gamma ray fluxes. However, its workability, adaptability, strength and low cost per unit of shielding are characteristics in its favor.

Tirpak (20) was first to study the feasibility of using high density concrete by utilizing barium sulfate aggregates known as barytes. This work was conducted at the Oak Ridge National Laboratories with the expectation of producing a heavy concrete having a shielding potential of 50 percent beyond that of ordinary concrete. Tirpak's investigation was successful in producing a mix criteria for a satisfactory heavy concrete (220 pounds per cubic foot). Based on his experiments, he reported that barytes concrete can be used for cell construction and for shielding purposes, provided it

is not submerged in water or exposed to continuous heavy washing action.

Properties of barytes aggregate

The better grades of barytes, obtained from Sweetwater, Tennessee, contain at least 90 percent $BaSO_4$. Table 1 (6) gives a partial chemical analysis of the aggregate. Table 2 (6) gives the gradation, density, specific gravity and the percent voids of the same aggregate. The higher concentration of iron in the fine aggregate is due to iron oxide Fe_2O_3.

The larger barytes aggregates, i. e. above 3/4 inch sizes, have a tendency to break up along cleavage planes. Thus under pressure this material will crumble into smaller pieces.

The finer aggregates, i. e. 3/4 inch maximum size have excellent strength. Hence when a mixture of the two aggregates (fine and coarse) is correctly chosen, a concrete of satisfactory strength may be produced.

Barytes is not found to contain or absorb appreciable amounts of water. In a recent publication from the Oak Ridge National Laboratories, Grantham (8) reported the following characteristics of barytes mined at Cartersville, Georgia:

a. Saturated-surface dry specific gravity 4.13

b. Saturated-surface dry H_2O content .85% by wt. of oven dry

Table 1. Partial chemical analysis of barytes aggregate

Component	Coarse Weight %	Fine Weight %
$BaSO_4$	95.9	81.6
Fe	1.0	9.8
Ca	.5	.9
O_2	1.3	6.2

Table 2. Physical properties of Sweetwater, Tennessee, barytes aggregates

Sieve Size	Coarse % Passing	Fine % Passing
1 inch	100	
3/4 inch	90-100	
3/8 inch	20-55	100
No. 4	0-10	95-100
No. 16		45-80
No. 50		10-30
No. 100		2-10
Weight per cu. ft.	162 lb. dry rodded	159 lb. dry rodded
Specific Gravity	4.2	4.0
Voids	38%	35%

c. Room dry water content .17 percent by weight of oven dry

d. Ratio of room-dry weight to saturated-surface dry weight .9933

Barytes obtained from the Western parts of the United States was found to contain alkali-reactive opal and chalcedony (6). These impurities react destructively in concretes containing high alkali cements and eventually cause the concrete to fail due to expansion cracks. Because of this it has been recommended (6) that all barytes aggregates be tested for these impurities. If they are found to contain more than .24 percent by weight opal and 5 percent by weight chalcedony, their use should be limited for use in low alkaline content cements.

Properties of barytes concrete

The physical properties of barytes concrete have been investigated and the results are available in U. S. Atomic

Table 3. Physical properties of barytes concrete

	Barytes	Ordinary
Density g/cm^3	3.5	2.3
Density lb./ft^3	218	144
Compression strength after 28 days psi	3500	3500
Thermal conductivity Btu/hr - ft ^oF at 200^oF	1.0	1.0
Specific heat Btu/lb. ^oF	.123	.156

Energy Commission publications. However, it might be mentioned here that barytes concrete has properties very much like ordinary concrete (6) as shown in Table 3.

EQUIPMENT

The equipment used in this investigation consisted of the following:

The Iowa State University radiation facility (14): this setup provided a fine beam of gamma rays (approximately 1/4 inch in diameter) from a 1.3 curie Co-60 source. The source is housed in a concrete block near the floor of the room. The source is raised by a motor, spur gear and rack apparatus into an upper cylindrical lead container 16 inches in diameter. This upper lead housing provided six beams of gamma rays, one of which was utilized for this investigation.

Single channel analyzer and scaler: for the detection of gamma ray spectrum a sodium iodide, thalium activated 1 inch in diameter by 1 inch deep scintillation crystal was used with model 1810 single channel analyzer and model 181-A scaler all made by Nuclear Chicago.

Collimater: a lead "brick" measuring 4x4x8 inches with a 1/4 inch diameter hole drilled through it was used to give a sharp gamma ray beam. This was done by allowing the emerging beam to pass through it before striking the barytes concrete block.

PROCEDURE

Determination of Scattering Properties of Barytes' Concrete

The main objective of this investigation was to observe in detail the gamma rays that are scattered at angles ranging from 20° to 75° measured from the direction of the incident beam. To facilitate this, two geometries were used as discussed below.

Geometry Ia

A 1.3 curie gamma beam approximately 1/4 inch in diameter was employed to strike a barytes concrete block measuring 2x2x4 inches. The sodium iodide (Th activated) crystal measuring 1 inch diameter by 1 inch deep was allowed to view 1/2 inch of the sample at every angle. This was accomplished by the use of lead blocks positioned as shown in Figure 4. At any given angle a plane of scattered radiation 1/2 inch wide reached the crystal.

Geometry Ib

The above geometry was kept constant, except that one other barytes concrete block was placed beside the first one. This is shown in Figure 5.

Geometry IIa

For this geometry the plane of radiation reaching the crystal was narrowed to 1/4 inch and the concrete block was altered. Its corner was rounded to a radius of 2 inches.

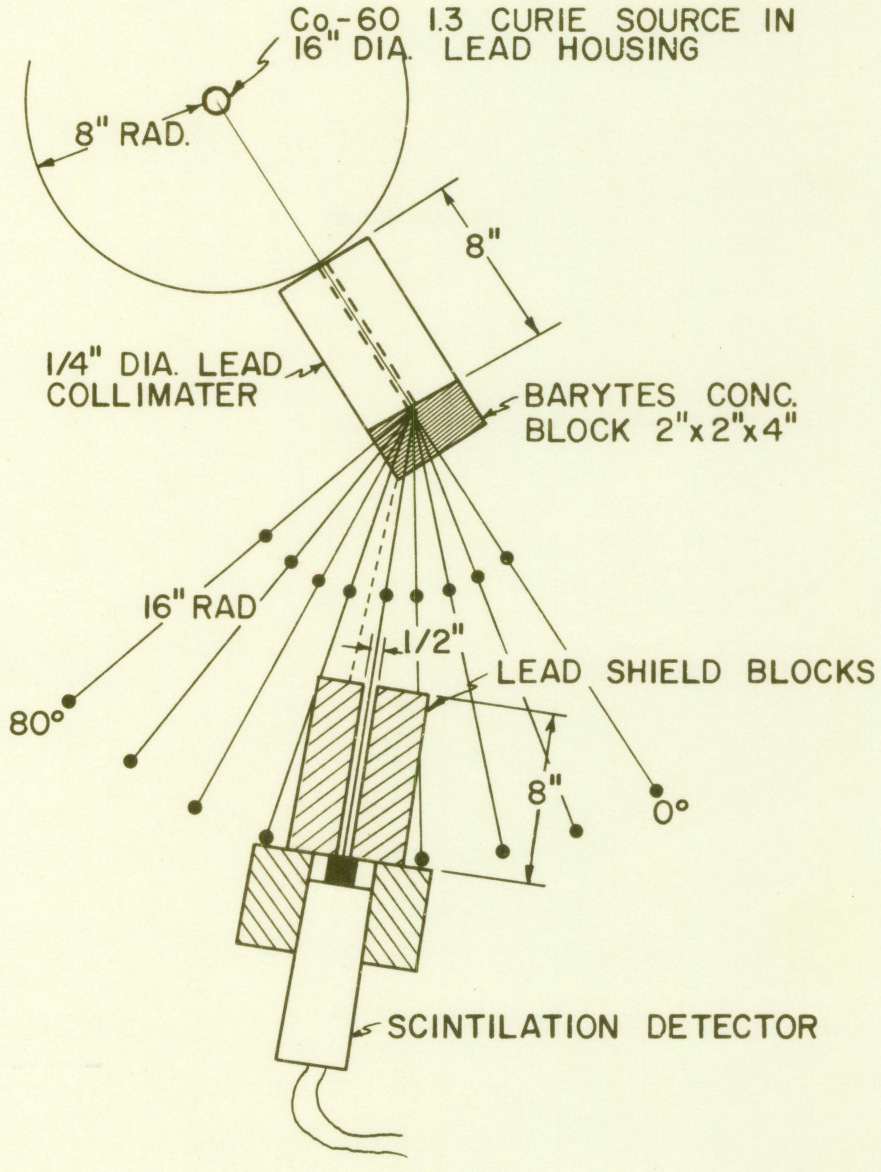

Figure 4. Geometry Ia

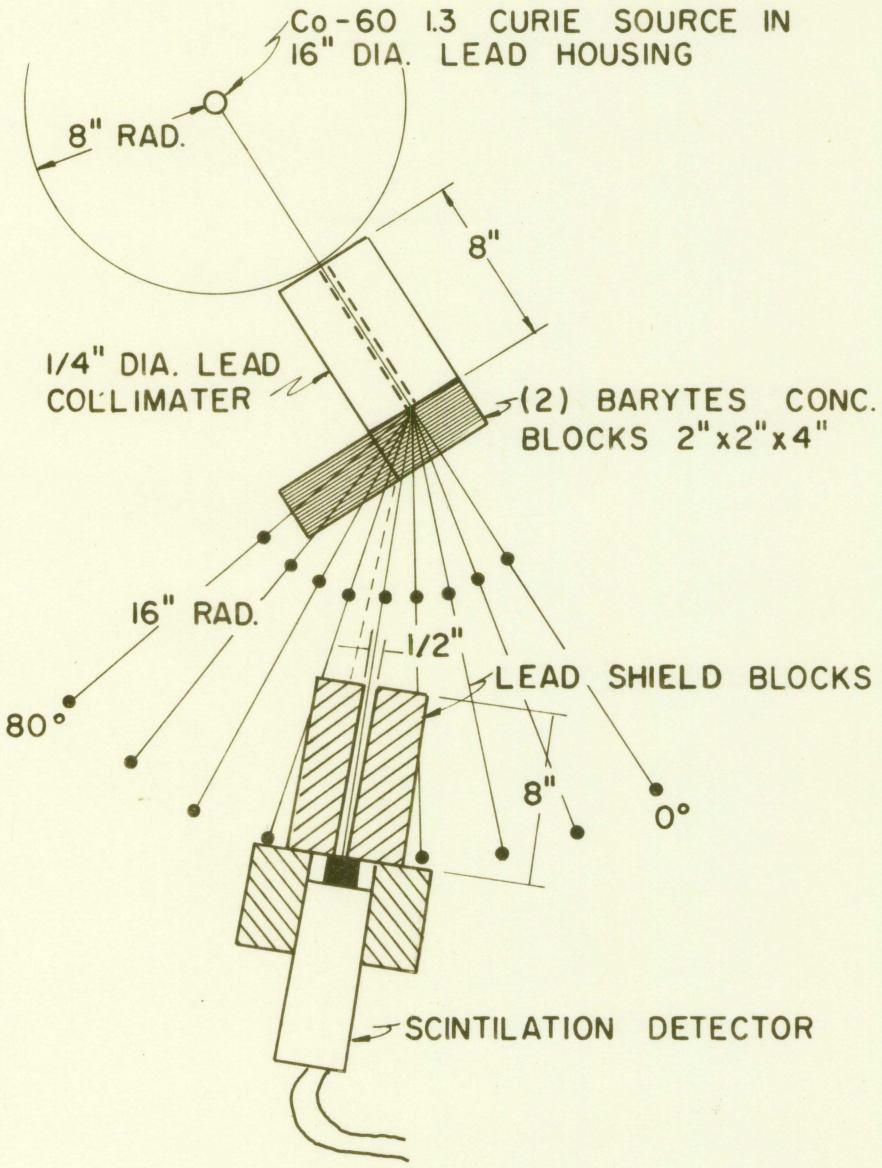

Figure 5. Geometry Ib

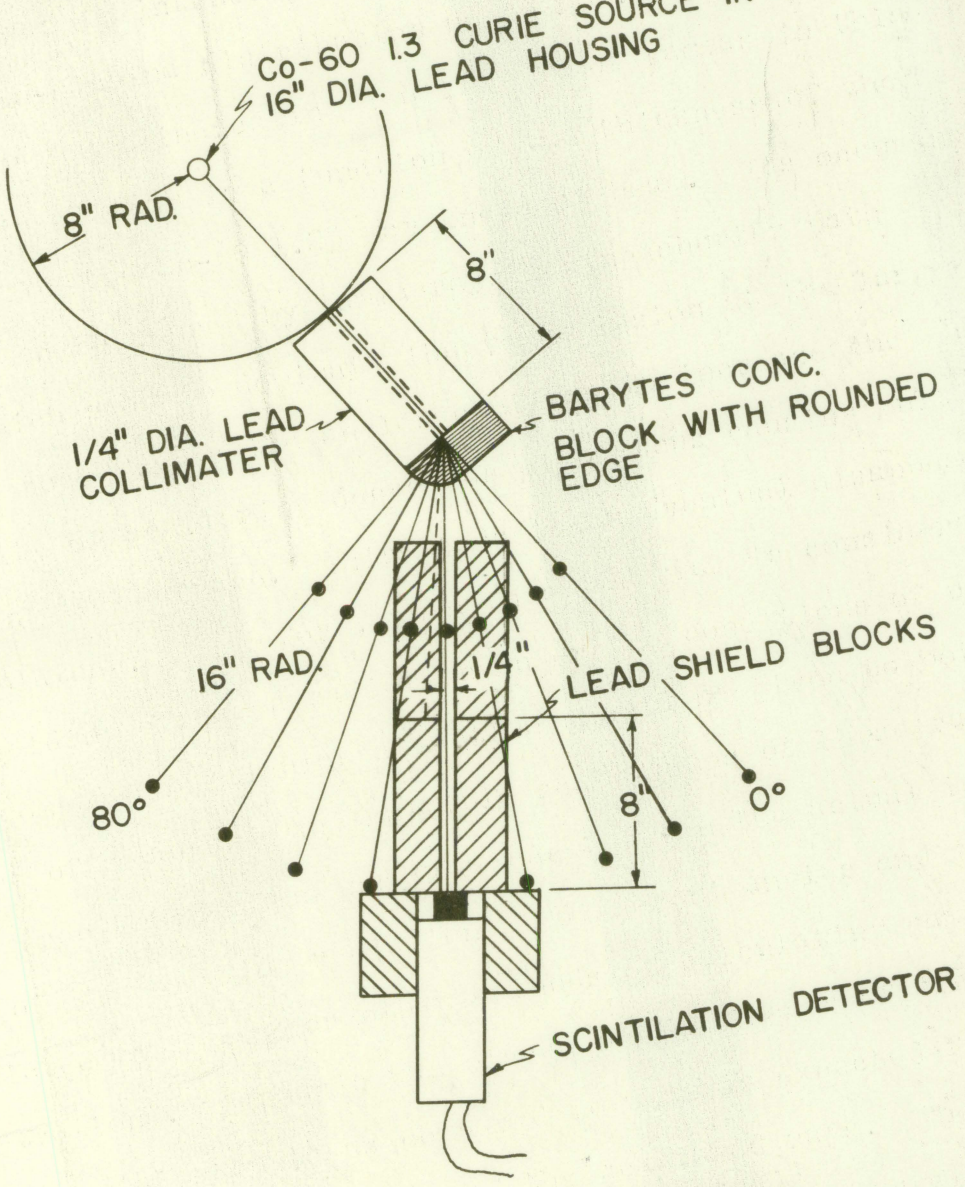

Figure 6. Geometry IIa

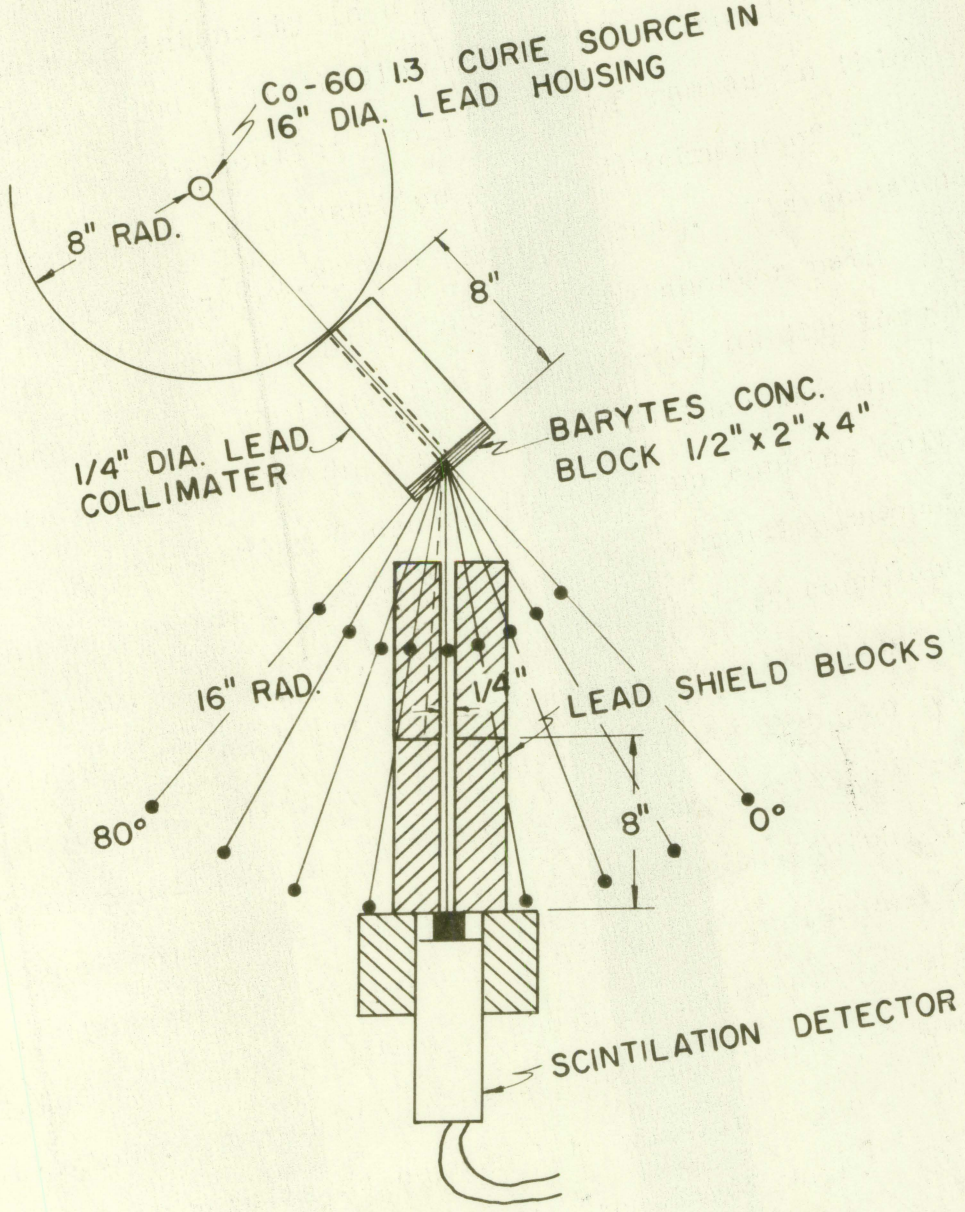

Figure 7. Geometry IIb

See Figure 6.

Geometry IIb

For this geometry the plane of radiation reaching the crystal was 1/4 inch and the concrete block was cut down to 1/2 inch thickness. See Figure 7.

For the above geometries, the total undiscriminated activity of the scattered gamma-ray beam was measured at angles from 20° to 80°. The activity was then plotted vs. angle on semi log paper.

The gamma ray energy spectrum was observed with the aid of a single channel analyzer at 10° intervals beginning with 20° and ending with 80°. The geometry used was essentially that of Geometry I. These results are shown in Figures 10 through 16.

The mass absorption coefficient of barytes concrete of density 3.4 gm/cm^3 was also determined. For this, seven blocks of this concrete were placed in a row and the total activity noted after each one was removed. These blocks were surrounded by lead walls on both sides. The geometry used was essentially that of Geometry II. The results of activity vs. absorber thickness are shown in Figure 17.

Evaluation of Background

The background activity was measured at every angle. This was done by blocking the channel of lead leading to the

crystal with a lead block, after removing the sample concrete block. Everything else was left unchanged for every geometry which was used.

Mix Criteria for the Barytes Concrete

In making the barytes concrete blocks the following factors were considered.

The use of small amounts of water and cement is necessary for high density concrete (6, 7, 20). These materials are less dense than barytes; therefore, they should not be used in more quantities than is necessary.

The use of large quantities of fine barytes is not recommended since this leads to an increase of surface area and would necessitate the use of more water and more cement to bind the mixture. All of these factors tend to reduce the density of the final mixture.

The exclusive use of coarse barytes is not recommended even though it increases the density. The larger aggregates show less strength and durability than the finer aggregates.

An effort was therefore made to combine the above opposing factors in order to give a satisfactory concrete mixture. The proportions used to make 24 blocks of 2x2x4 inches size were as follows:

Type one cement (15)	4 pounds
Sweetwater, Tennessee barytes aggregates	42 pounds

Water 2.3 pounds

This gave a concrete of density 3.4 gm/cm^3 and of compression strength 2500 psi. The difference in water content between samples placed in 100 percent environment and those at ordinary room conditions was approximately 2 percent.

Table 4 shows the sieve analysis of the aggregates used.

Table 4. Sieve analysis

Sieve size	% Retained	% Passing
3/4 inch	0	100
3/8 inch	33.8	66.2
No. 4	40.8	59.2
No. 8	57.9	42.1
No. 16	74.3	25.7
No. 30	87.1	12.9
No. 50	92.7	7.3
	99.7	0.3

RESULTS AND ANALYSIS OF DATA

Plateau Formation

As stated in the procedure, two main geometries were used to examine the scattered gamma rays through angles of 20° to 80° from the direction of the incident 1.3 curie Co-60 gamma beam. Curve 1 of Figure 8 shows the result for Geometry Ia. An examination of this curve reveals that the total undiscriminated activity decreases along a straight line from 20° to 40°. Between 40° and 60° a flat region develops. Beyond 60° the curve drops along a straight line until an angle of 75° is reached.

Recalling that the barytes concrete block measured 2x2x4 inches and that its corners were situated at 45° to either side of the incident beam, one might hasten to associate this corner with the occurence of the plateau. One might also observe that at 45° the oblique distance from the point at which the incident beam strikes the block to where scattered photons emerge is a maximum. Hence the plateau could be attributed to build up as well.

Such speculations led to Geometry Ib which eliminated the corner effect at 45°, Figure 5. Here, as was pointed out before, another concrete block was placed adjacent to the first one used. The result of this change is indicated by Curve 2 of Figure 8. This curve shows a similar but smaller plateau up to 55°. Beyond 55° it drops much faster than

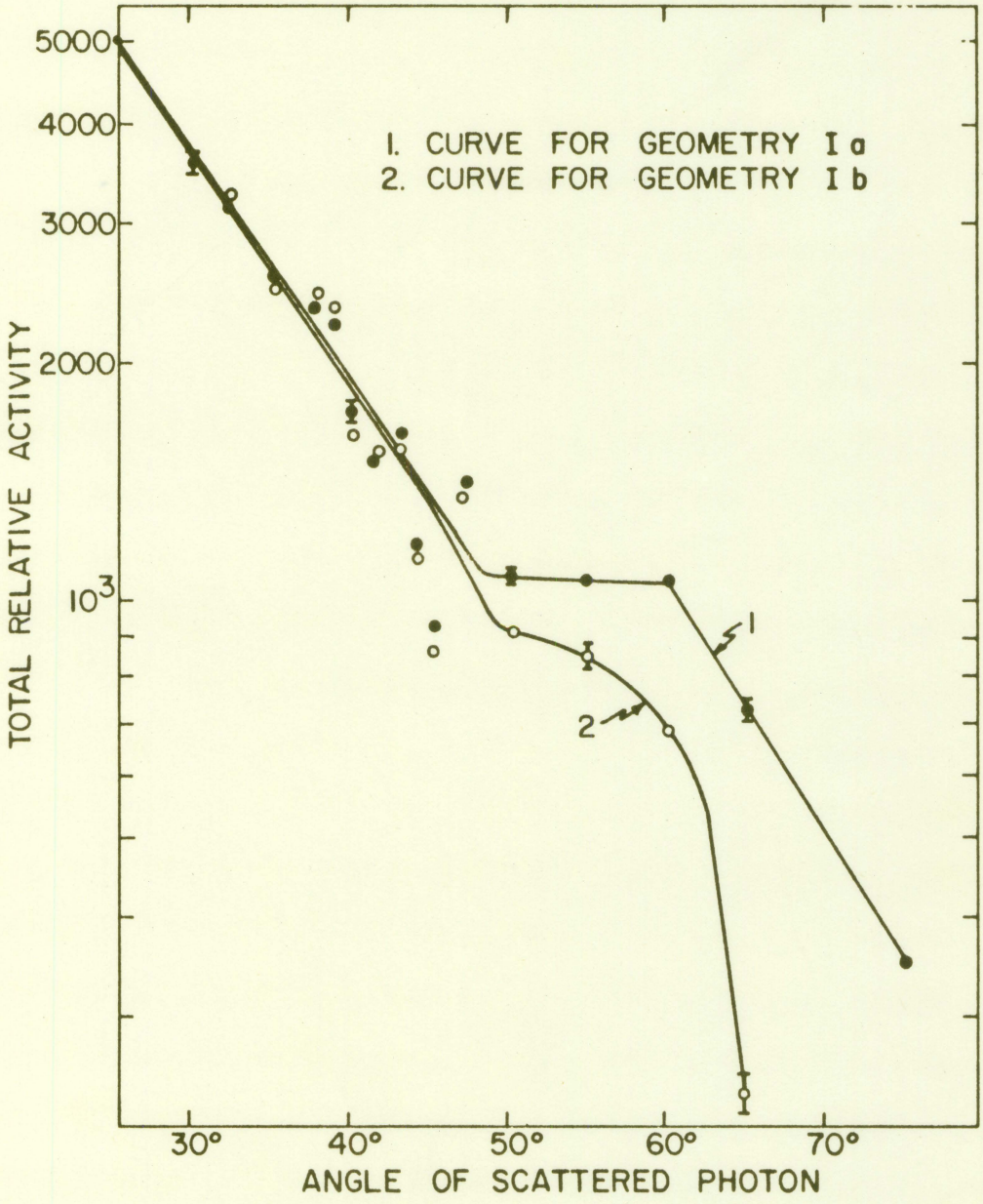

Figure 8. Results of Geometry Ia and Geometry Ib

Curve 1 due to an increase in the oblique distance. It might be noticed that the two curves coincide at angles below 45° as expected.

Comparison of the trend of the results obtained up to this point with the theoretical predictions indicated by Klein and Nishina in Nelms (16) may be obtained by plotting Curves 1 and 2 of Figure 8 on polar coordinates. Such comparisons are justified due to the fact that the activity obtained is proportional to the cross section. Another comparison may be made directly by referring to Figure 2 which shows a plot of the differential cross section per electrons vs. angle (16). In any case, such comparisons show that the occurance of the plateau is not predicted by the Klein-Nishina equation. Since the Klein-Nishina equation does not account for multiple scattering, the differences in the shapes of the curves gives an indication of this multiplicity in scattering. The results of Geometry Ib excluded corner effects as a possible reason for plateau formation, there remains the oblique distance variance and the build up associated with it to be considered.

Geometry IIa eliminates oblique distance variance and any change in build up associated with it, by virtue of the fact that the corner was rounded to a radius of 2 inches. More attention was given here to screening out any possible scatter from other parts of the block by first allowing a plane of radiation 1/4 inch wide to reach the crystal and by increasing the length of the lead channel from 8 inches to 16 inches. The

results obtained are shown by Curve 1 of Figure 9a.

The fact that the plateau occurred here also might lead one to speculate that the thickness of the concrete block may be involved. Thus we are led to Geometry IIb where the thickness of the sample was reduced from 2 inches to 1/2 inch, everything else was identical with Geometry IIa.

The result of this is shown by Curve 2 of Figure 9a. This curve does not show a plateau. Therefore, unless the plateau is a result of some effect not included in this study, it is logical to conclude that it is a function of thickness of the block within the limits of the geometries used.

As thickness of the block increases, the number of scattered photons having shorter path lengths increase also. Path lengths are defined here to mean the distance between collisions that any photon might undertake. These photons show an increase in the transmitted radiation between 40° and 60°. This increase may come about because of the following reasons. First, at small angles, i. e. angles between 0 and 35°, the transmitted radiation is high. The secondary photons, i. e. those having shorter path lengths do not contribute enough radiation to change the shape of the curve in this region appreciably. Secondly, at larger angles, i. e. those beyond 60°, the probability of an initial scattering decreases according to the Klein-Nishina distribution shown in Figure 3. This fact causes the secondary collisions at those angles to decrease also. Therefore we are left with a region between

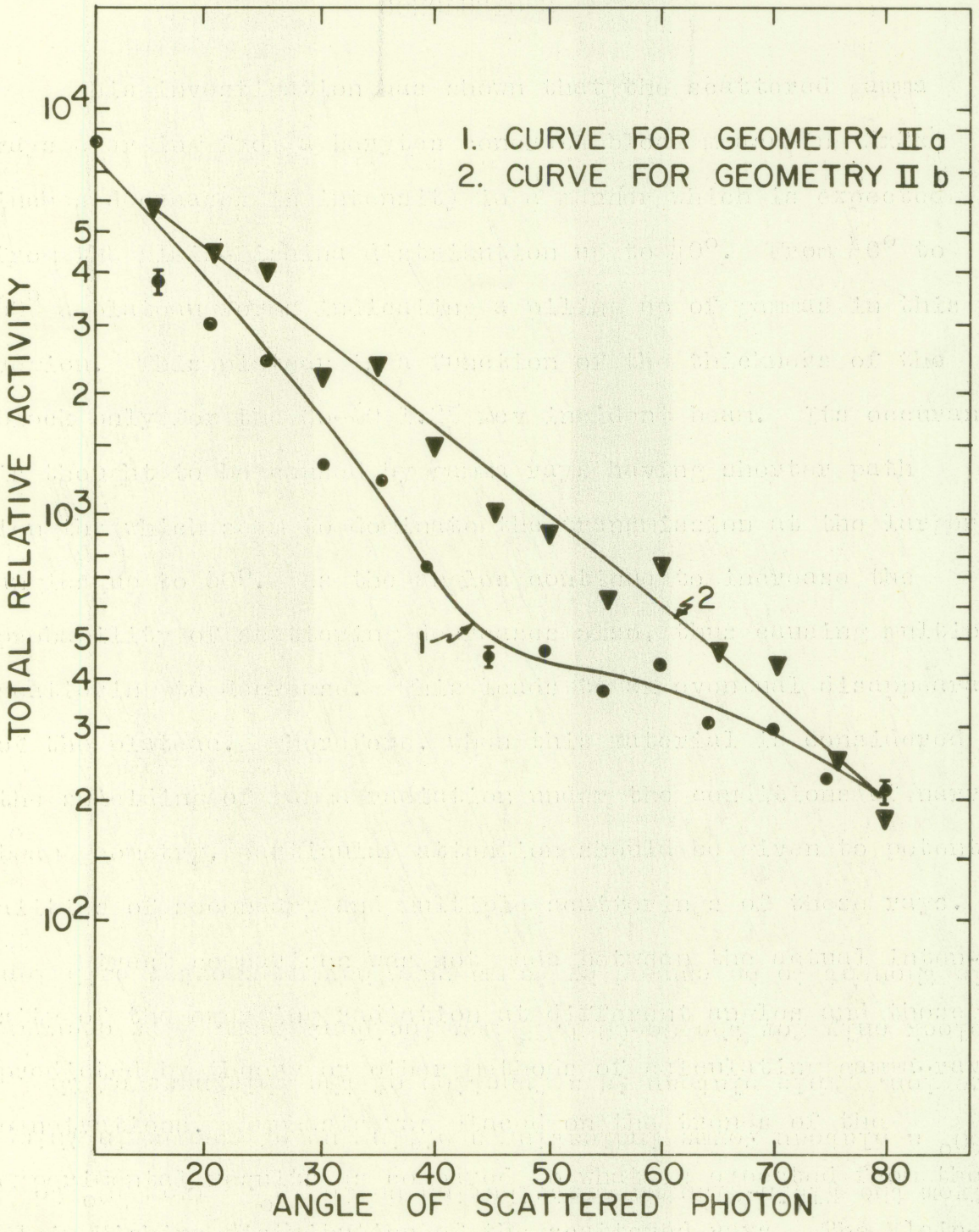

Figure 9a. Results of Geometry IIa and Geometry IIb

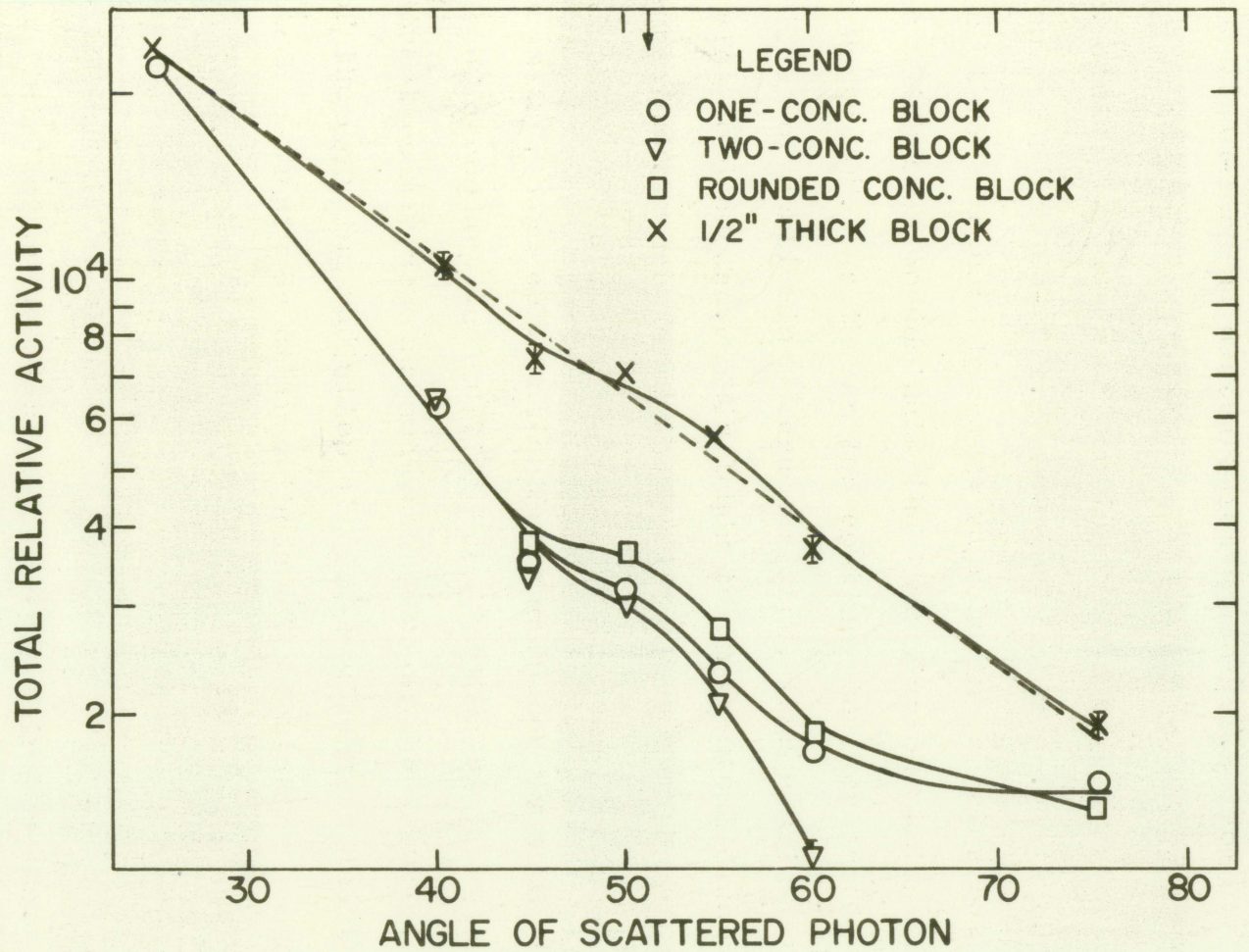

Figure 9b. Relative intensity distribution of scattered photons vs. angle for all four configurations

these two extremes where the secondary photons seem to dominate the transmission to a degree high enough that it could be detected.

The results obtained for the gamma-ray spectrum at 45°, 50° and 60° support the above explanation. Here we notice that the relative peaks of the normalized spectrum-curves do not fall off as one might expect from the Klein-Nishina distribution. Some stagnation or piling up of gamma photons is evident at these angles. This fact seems to indicate that some primary photons are being scattered down into this energy range thus contributing to the amount of transmitted radiation.

When the significance of some of the experimental points in Figure 8 and Figure 9a seemed critical in the determination of the plateau, the scattering at different angles was measured again. The set up used was similar to that of Geometry II except for the distance between the detector and the concrete block. This distance was decreased so that a higher count rate may be obtained. One concrete block, two concrete blocks, a rounded edge concrete block and the 1/2 inch concrete block were placed in the path of the gamma beam in succession. Thus four points were obtained per angle from 25° to 75°. The resulting curves are shown in Figure 9b. These are in agreement with what has been discussed previously. All curves show a plateau except the 1/2 inch sample where the curve is almost a straight line.

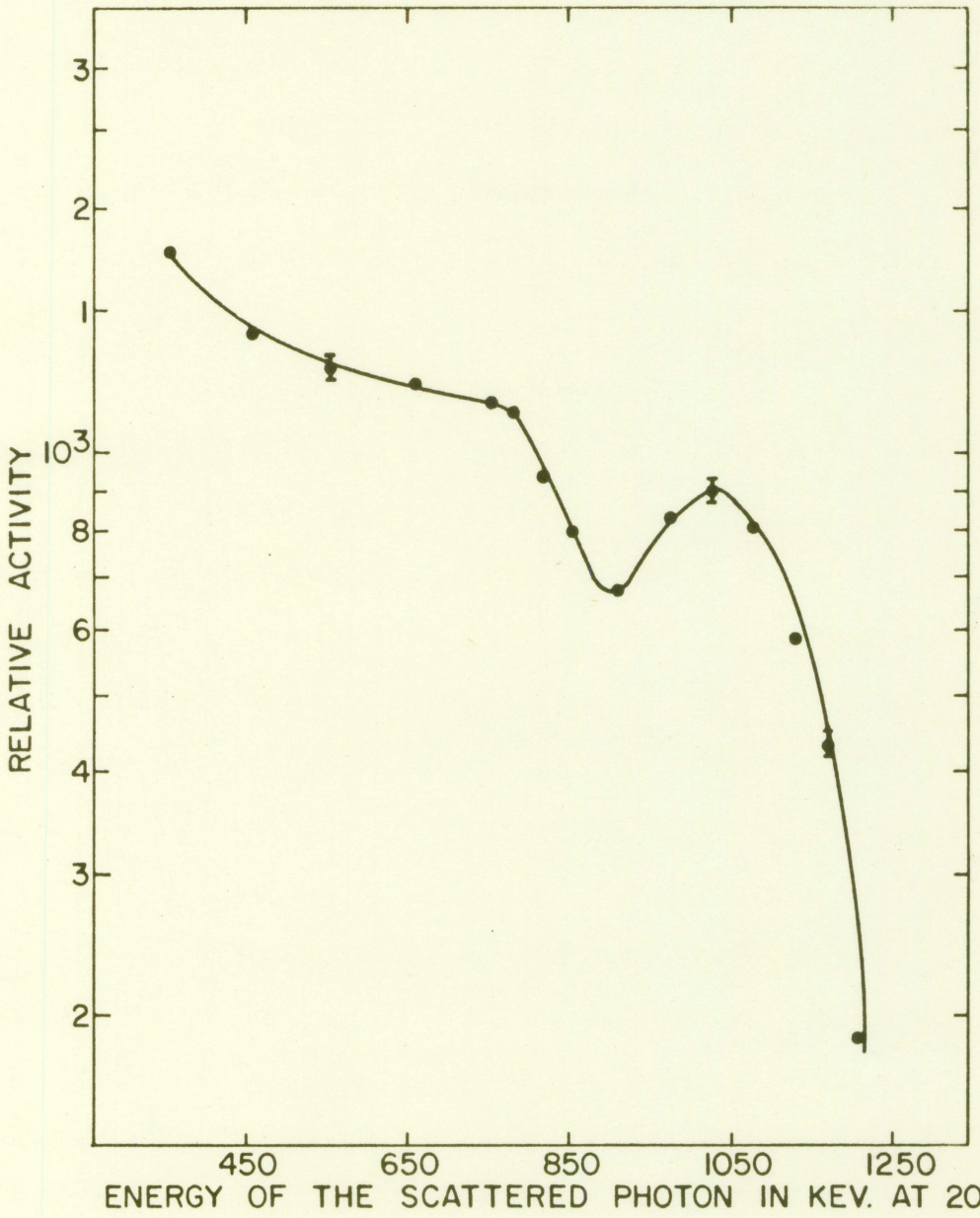

Figure 10. The scattered gamma-ray spectrum at 20°

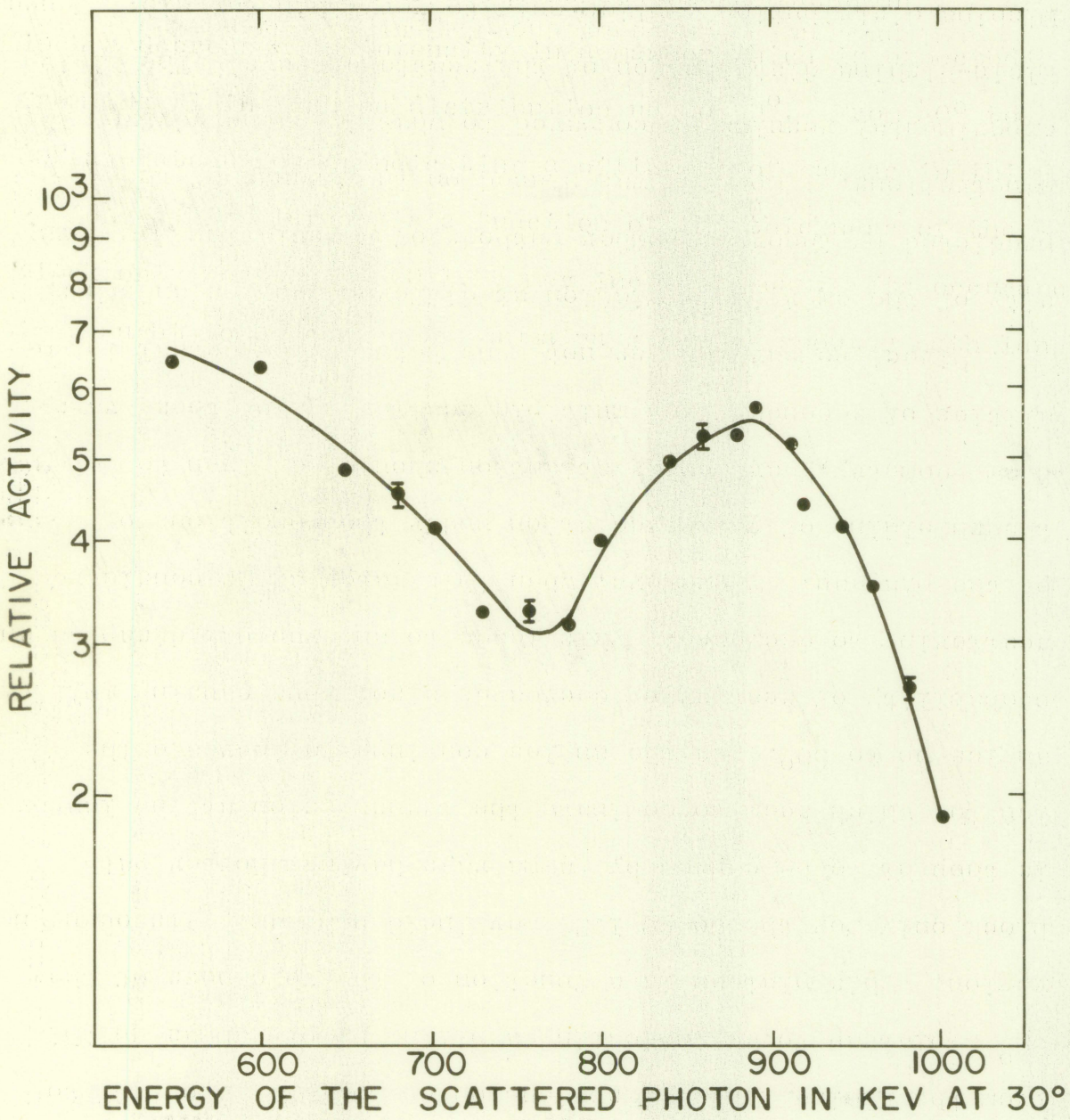

Figure 11. The scattered gamma-ray spectrum at 30°

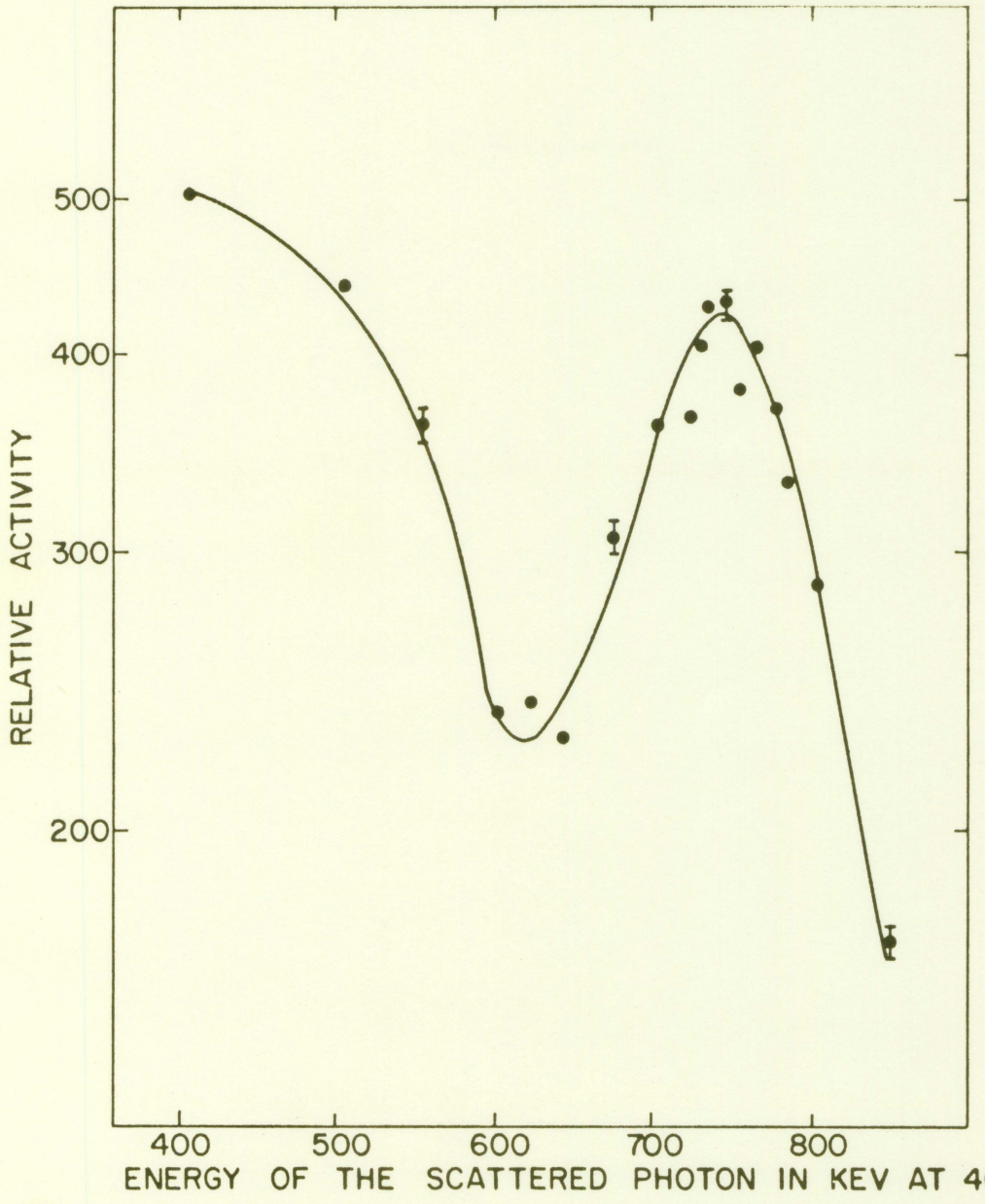

Figure 12. The scattered gamma-ray spectrum at 40°

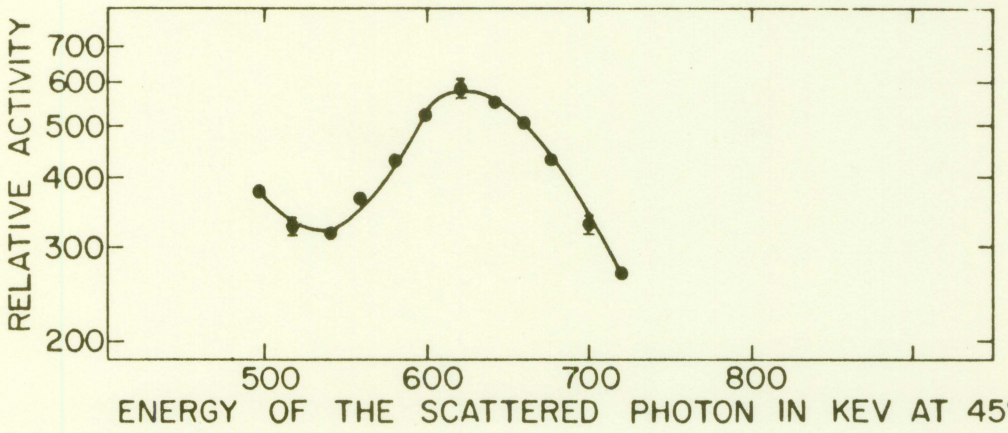

Figure 13. The scattered gamma-ray spectrum at 45°

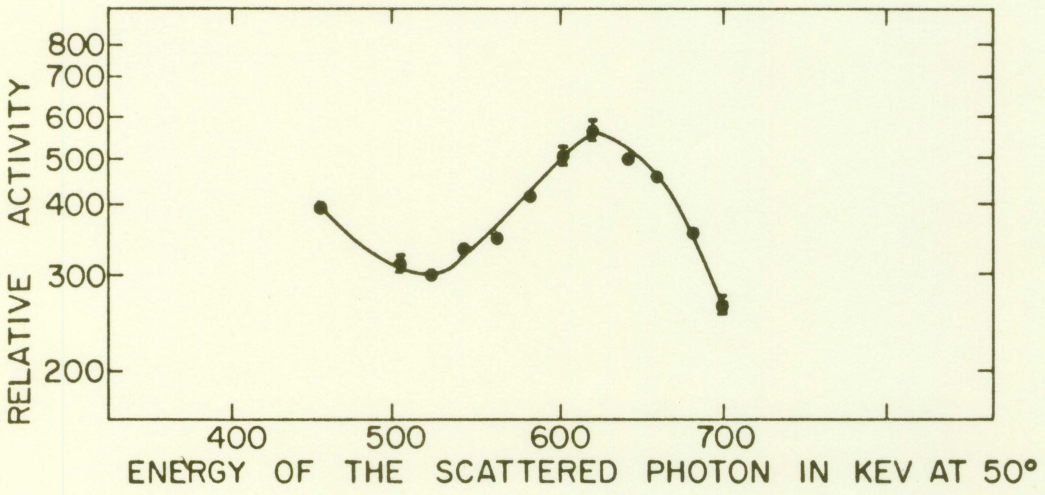

Figure 14. The scattered gamma-ray spectrum at 50°

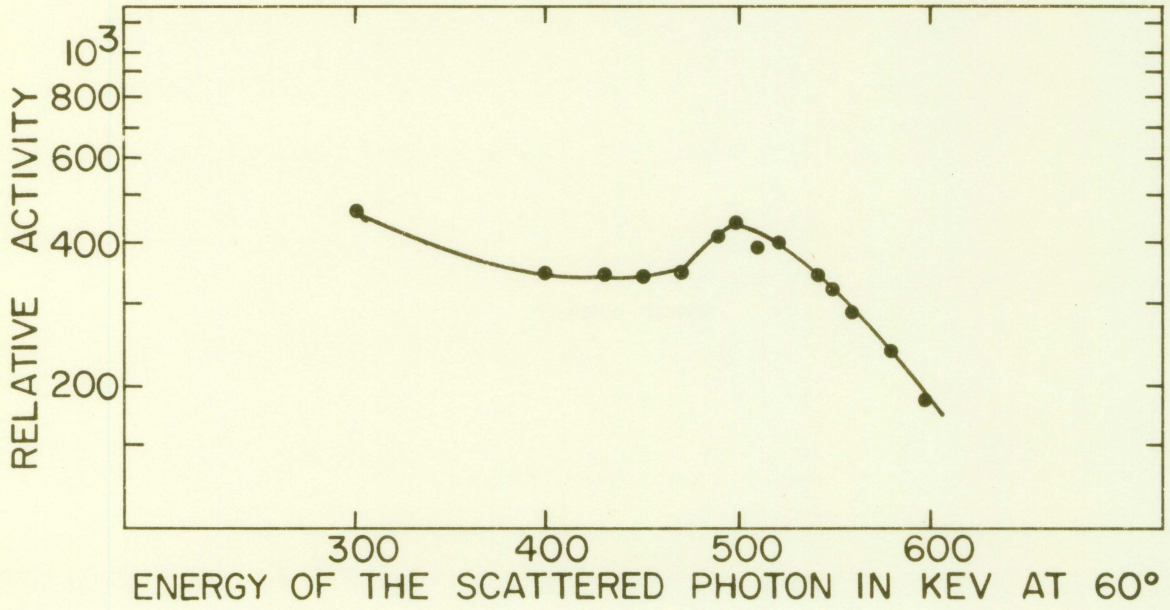

Figure 15. The scattered gamma-ray spectrum at 60°

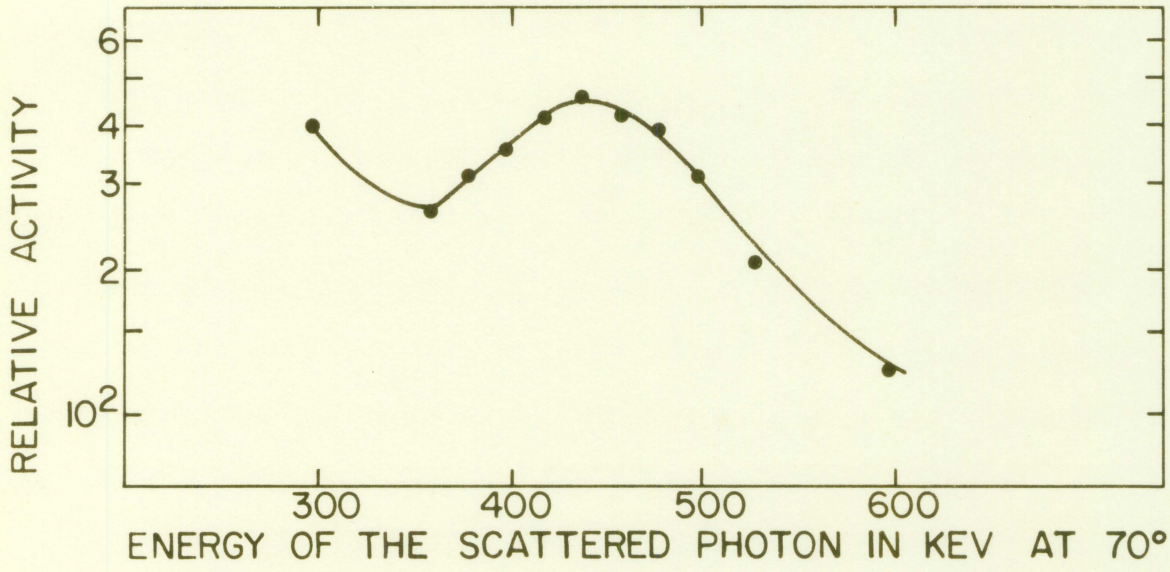

Figure 16. The scattered gamma-ray spectrum at 70°

Spectrum of the Scattered Photon

Utilizing the Geometry Ia, the scattered gamma energies were found with the aid of a single channel analyzer. The results are shown in Figures 10 through Figure 16.

Table 5 shows the experimental peak energies at 10° intervals from 20° to 70° as well as the calculated peak energies from the equation

$$E^1 = \frac{E}{1 + \frac{E}{mc^2}(1 - \cos\theta)}$$

where E^1 is the energy of the scattered photon, E is the energy of incident photon taken as 1.25 mev for Co-60 and θ is the angle the scattered photon makes with the incident photon.

As may be seen, the experimental results are in agreement with what is predicted by the Compton scatter equation.

The significance of this part of the investigation lies in the fact that while we are not able to use the differential cross section per electron to predict accurately the behavior of the scattered photons due to multiple interactions of the photons, we find that the measured peak energies at these angles as well as all others to be almost in perfect agreement with theory.

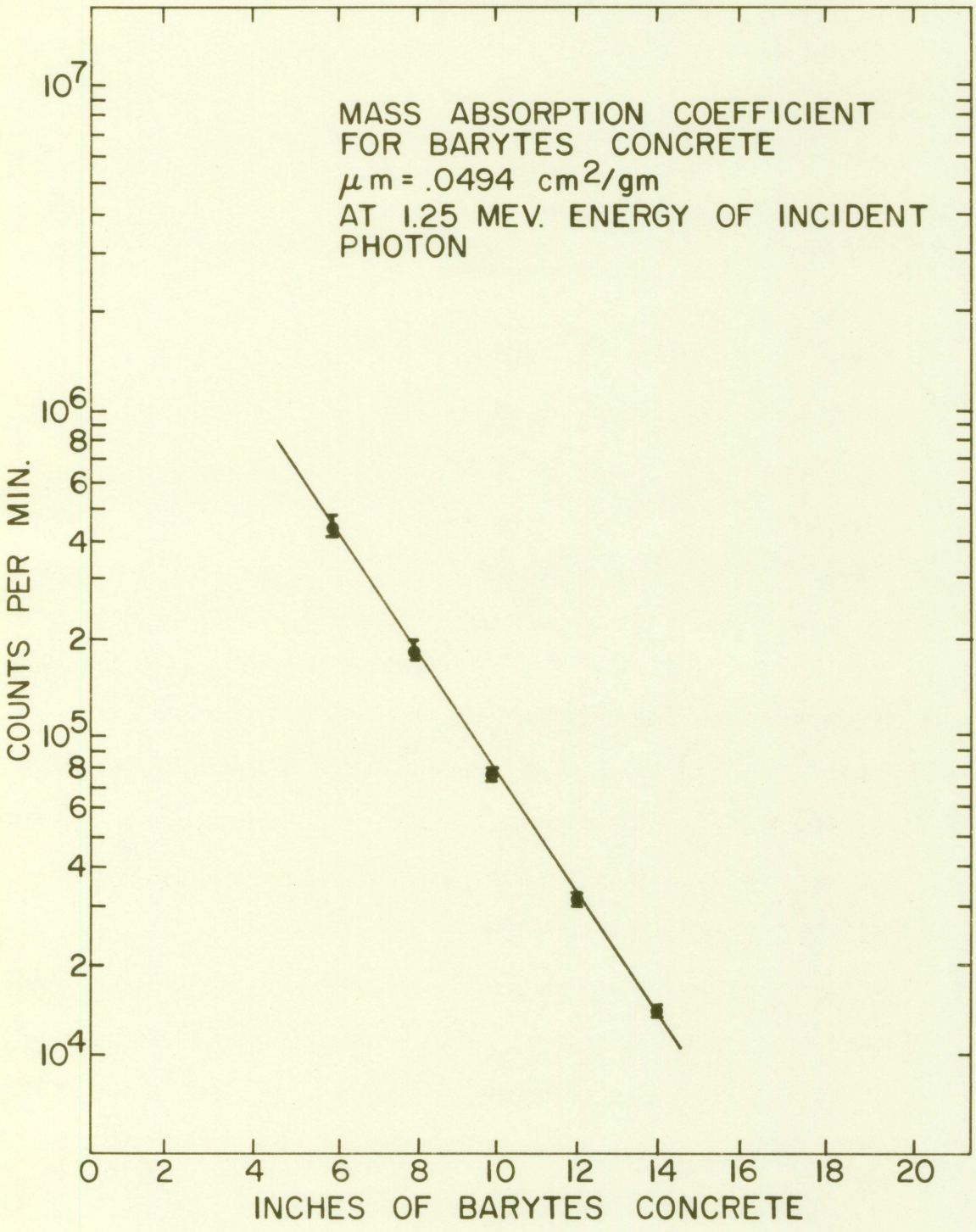

Figure 17. Counts per minute vs. absorber thickness

Table 5. Calculated and observed scattered photon peak energies

Angle in degrees	Calculated peak in kev	Measured peak in kev
20	1087	1030
30	936	915
40	788	765
45	723	695
50	660	645
60	555	525
70	472	455
80	408	405

Mass Absorption Coefficient

The mass absorption coefficient μ_m in cm^2 per gram is always important in radiation attenuation calculations. For barytes concrete it has the value of .05 cm^2/gm.

This value was arrived at from the slope of Figure 17 which represents counts per minute vs. absorber thickness in inches of barytes concrete. The value .05 cm^2/gm was obtained consistently when several runs were taken with different blocks selected at random from a total of 24 blocks. Walker (21) reports a value of approximately .052 for a barytes concrete of density 3.39 gm/cm^3 which is in good agreement with that determined here.

CONCLUSIONS

This investigation has shown that the scattered gamma rays emerging from a barytes concrete block measuring 2x2x4 inches decreases in intensity in a manner which is expected from the Klein-Nishina distribution up to 40°. From 40° to 60° a plateau forms indicating a piling up of gammas in this region. This plateau is a function of the thickness of the block only for the Co-60 1.25 mev incident beam. Its occurance is thought to be caused by gamma rays having shorter path lengths which seem to dominate the transmission at the larger angles up to 60°. As the angles continue to increase the probability of scattering decreases also, thus causing multiple scattering to decrease. This leads to an eventual disappearance of the plateau. Therefore, when this material is considered for the shielding of gamma radiation under the conditions of narrow beam geometry, particular attention should be given to potentialities of secondary and multiple scatterings of these rays.

Direct comparison was not made between the actual intensity of the emerging radiation at different angles and those predicted by theory or other methods of calculating gamma-ray penetrations. Emphasis was placed on the trends of the experimental results as compared to what is expected from the Klein-Nishina distribution of the scattered rays. The Klein-Nishina distribution applies only to very thin targets. Hence the deviations observed by examining the relative peak heights

of the spectrum curves is a measure of the extent of the deviations from purely theoretical considerations. These same deviations are reflected in the formation of the plateau.

BIBLIOGRAPHY

1. Avery, A. F. Methods of calculation for use in the design of shields for power reactors. U. S. Atomic Energy Commission Report. [Gt. Britain Atomic Energy Research Establishment, Harwell, Berks., England.] May, 1960.

2. Binner, C. R. High density concrete shielding. U. S. Atomic Energy Commission Report HFK-1. [Ferguson (H. K.) Co., New York]. February, 1949.

3. Compton, Arthur H. X-rays and electrons. New York, N. Y., D. Van Nostrand Co. 1926.

4. Crouthamel, C. E. Applied gamma-ray spectrometry. New York, N. Y., Pergamon Press. 1960.

5. Fermi, E. Nuclear physics. Revised edition. Chicago, Ill., The University of Chicago Press. 1950.

6. Gallaher, R. B. and Kitzes, A. S. Summary report on portland cement concretes for shielding. U. S. Atomic Energy Commission Report ORNL-1414. [Oak Ridge National Lab., Tenn.]. March, 1953.

7. Goldstein, H. and Wilkins J. E. Calculations of the penetration of gamma rays. U. S. Atomic Energy Commission Report NYO-3075. [New York Operation Office, AEC]. June, 1954.

8. Grantham, W. J. Barytes concrete for radiation shielding: Mix criteria and attenuation characteristics. U. S. Atomic Energy Commission Report ORNL-3130. [Oak Ridge National Lab., Tenn.]. June, 1961.

9. Green, Alex. Nuclear physics. New York, N. Y., McGraw-Hill Co., Inc. 1955.

10. Grotenhuis, M. Lecture notes on reactor shielding. U. S. Atomic Energy Commission Report ANL-6000. [Argonne National Lab., Lemont, Ill.]. March, 1951.

11. Heitler, W. The quantum theory of radiation. Oxford, England, The Clarendon Press. 1936.

12. Jaeger, T. Concrete, the convenient reactor shielding material. Atomic World. 9:416-418. 1958.

13. Lapp, Ralph E. Nuclear radiation physics. 2nd ed. Englewood Cliffs, N. J., Prentice-Hall, Inc. 1955.

14. McDermott, M. A. An irradiation facility with a two-curie Co-60 source. Unpublished M.Sc. thesis. Ames, Iowa, Library, Iowa State University of Science and Technology. 1958.

15. Murphy, Glenn. Properties of engineering materials. 3rd ed. Scranton, Pa., Internation Textbook Co. 1957.

16. Nelms, Ann. Graphs of the Compton energy-angle relationship and the Klein-Nishina formula from 10 kev to 500 mev. National Bureau of Standards Circular 542. 1953.

17. Richtmyer, F. K. Introduction to modern physics. 3rd ed. New York, N. Y., McGraw-Hill Co., Inc. 1942.

18. _____. Introduction to modern physics. 5th ed. New York, N. Y., McGraw-Hill Co., Inc. 1955.

19. Ruddy, John M. Gamma ray shielding for engineering reference. U. S. Atomic Energy Commission Report AECU-1211. [Technical Information Service Extension, AEC]. February, 1951.

20. Tirpak, E. D. Report on the use of barytes concrete in shielding. U. S. Atomic Energy Commission Report ORNL-665. [Oak Ridge National Lab., Tenn.]. 1951.

21. Walker, R. L. and Grotenhuis, M. A summary of shielding constants for concrete. U. S. Atomic Energy Commission Report ANL-6443. [Argonne National Lab., Lemont, Ill.]. November, 1961.

ACKNOWLEDGEMENTS

I wish to thank Dr. Murphy for introducing this topic, Professor Sasscer, Professor Chamberlin and Mr. Heiskala for their help and useful suggestions which made the completion of this project possible.